THE GEOLOGICAL SOCIETY OF AMERICA®

CONNECTS 2021

10–13 October
Portland, Oregon, USA

Relative roles of impact-generated aerosols on photosynthetic activity following the Chicxulub asteroid impact

Cem Berk Senel(1,*), Orkun Temel(2,1), Pim Kaskes(3,4), Johan Vellekoop(3,5), Steven Goderis(3), Bart Van Hove(6) and Ozgur Karatekin(1)

(1) Reference Systems and Planetology Department, Royal Observatory of Belgium, Belgium
(2) KU Leuven, Institute of Astronomy, Leuven, Belgium
(3) Analytical, Environmental, and Geochemistry, Vrije Universiteit Brussel, Belgium.
(4) Laboratoire G-Time, Université Libre de Bruxelles, Belgium
(5) Department of Geology, KU Leuven, Leuven, Belgium
(6) Deimos Space, Madrid, Spain

(*)Corresponding author, email: cem.berk@observatory.be

Motivation: simulating the aerosol-driven climatic response to Chicxulub impactor

Our main focus → K-Pg impact winter conditions and assessing the cessation of photosynthesis in terms of the photosynthetically active radiation (PAR).

Table 1:

asteroidImpactWRF

Land-surface physics, microphysics, cumulus convection
Boundary-layer turbulence (Senel et al., 2019) → **planetWRF-core** (Richardson et al. 2007)

↓

Asteroid impact dynamic model ← Impact event

- **Aerosol microphysics module**
  - Sulfur
    - Wet deposition (Feichter et al., 1991)
    - Dry deposition (Feichter et al., 1996) + (Xu, Charmichael, 1998)
  - Dust
    - Wet deposition (Tsarpolis et al., 2018)
    - Two-moment dry deposition (Binkowski & Shankar, 1995) (Zhang & Shao, 2014) (Senel et al., 2021)
    - Spectral dust lifting (Shao et al., 2001, 2004, 2009, 2010, 2011)
  - Soot (Black Carbon)
    - Wet deposition (Tsarpolis et al., 2018)
    - Two-moment dry deposition (Binkowski & Shankar, 1995) (Zhang & Shao, 2014) (Senel et al., 2021) + (Toon et al., 2016)
- **Aerosol radiation module** + Goddard Radiation Scheme
  - Sulfur SW, Sulfur LW (Kiehl and Briegleb, 1993)
  - Dust SW → (Feng et al., 2015)
  - Dust LW → (Dufresne et al., 2002)
  - Soot (BC) SW, Soot (BC) LW (Hess et al., 1998) (Kaiho et al., 2016)

General Circulation Model (GCM) set-up

- GCM simulations are performed by in-house asteroidImpactWRF model [Senel et al., 2021] based upon planetWRF framework [Richardson et al., 2007].
- Late Cretaceous paleogeography is based on [Markwick and Valdes, 2004]. Model land albedo values are determined using the plant functional type map from [Niezgodzki et al., 2017].
- The horizontal model resolution is 5° over the zonal and meridional directions, having 27 vertical sigma layers extending through upper stratosphere.
- Goddard radiation model [Chou and Suarez, 1999, Chou et al., 2001] is used for the shorthwave and longwave radiative transfer.
- The aerosol (dust, sulfur, soot) microphysics (lifting, dry/wet deposition) and radiation is modeled as given in Table 1.
- Boundary-layer turbulence is modeled by a recent PBL scheme [Senel et al., 2019].
- For the parameterization of microphysical processes, Purdue-Lin microphysics scheme is used [Chen and Sun, 2002].
- 5–layer thermal diffusion scheme is utilized for land-surface physics [Dudhia, 1996], the surface layer is modeled by the revised MM5 scheme [Jiménez et al., 2012].
- Cumulus parameterization is treated by the modified Tiedtke scheme [Tiedtke, 1989, Zhang et al., 2011].
- For the ocean model, one-dimensional ocean mixed layer model (OMLM) is used [Pollard et al., 1973].

Description of GCM experiments: Chicxulub impact scenarios

- In the present study, we perform three impact scenarios based on the aerosol type:
  - 1. Dust
  - 2. Sulfur
  - 3. Fine soot
- GCM simulations are performed for the Late Cretaceous climate conditions taking the globally-averaged atmospheric CO_2 concentration to be nearly 560 parts per million (ppm), similar to [Brugger et al., 2017, Tabor et al., 2020].
- For orbital parameters, circular orbit with an obliquity of 23.5° is assumed [Brugger et al., 2017].
- The solar constant is taken to be $\sim$1354 W/m^2 based on [Brugger et al., 2017], similar to [Niezgodzki et al., 2017, Tabor et al., 2020].
- The impact time, thus aerosol generation, is assumed to be occurred in early northern spring (in March).
- Time integration for each impact simulation is carried out for 20 years where the first 5-years are omitted (initial spin-up).

2.1. Impact-driven aerosol injection: Dust

13188 **O. B. Toon et al.: Designing climate and chemistry simulations for asteroid impacts**

Table 1. K-Pg injection scenario for impactor mass $\sim 1.4 \times 10^{18}$ g; impact energy $\sim 2.8 \times 10^{23}$ J $= 6.8 \times 10^{7}$ Mt for 20 km s^{-1} impact.

Property/ constituent	Type 2 spherules	Soot	Nanoparticles	Clastics, < µm	S
Material amount, g, column density (g cm^{-2})	2.3×10^{18} (0.44)	1.5–5.6×10^{16} (0.29 to 1.1×10^{-2})[c]	$\sim 2 \times 10^{18}$[b] (0.4)	$< 6 \times 10^{16}$ (0.01)	9×10^{16} (5×10^{-2} g cm^{-2} as SO_4)
Global optical depth as 1 µm particles[a]	~20 (for 250 µm particles)	~100	~2000	~90	~450
Vertical distribution	70 km, Gaussian distribution with half width of 6.6 km[d]	Eq. (2)	Same as Type 2 spherules	Uniformly mixed vertically above tropopause	Same as Type 2 spherules
Optical properties	Not relevant	$n = 1.8$ $k = 0.67$	Hervig et al. (2009)	Orofino et al. (1998) limestone	Sulfuric acid
Initial particle size	250 µm diameter	Lognormal, $r_m = 0.11$ µm, $\sigma = 1.6$; monomers 30–60 nm	20 nm diameter	Lognormal, $r_m = 0.5$ µm, $\sigma = 1.65$	Gas
Material density, g cm^{-3}	2.7	1.8	2.7	2.7	1.8

[a] Qualitative estimate for comparison purposes only. [b] This value is an upper limit. The lower limit is zero. [c] These values are for aciniform soot or elemental carbon in the stratosphere (see text). [d] The material may have quickly moved to below 50 km to maintain hydrostatic balance (see text).

Mass of injected dust → m_a = 2,000,000 Tg (Toon et al. 2016)

- **Initial dust particle size**
  d_p = 250 µm is given in Toon et al. 2016.

  We assumed poly-dispersed dust particles:
  as a log-normal distribution two-moment dust transport scheme

$$n_N(D_p)dD_p = \frac{1}{\sqrt{2\pi} D_p ln\sigma_{g,0}} exp\left(-\frac{(lnD_p - lnD_{pg,0})^2}{2ln^2\sigma_{g,0}}\right)$$

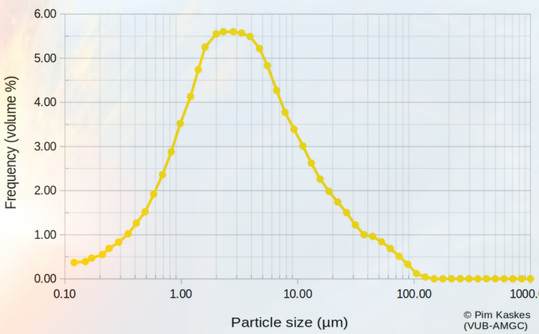

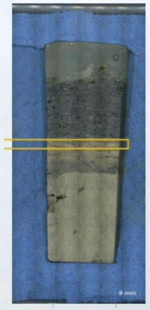

constrained by the laser-diffraction grain-size analysis of clay-rich KPB sediments from a recent field study in North-Dakota, by VUB - Analytical, Environmental & Geo-Chemistry group.

Toon, O. B., Bardeen, C., & Garcia, R. (2016). Designing global climate and atmospheric chemistry simulations for 1 and 10 km diameter asteroid impacts using the properties of ejecta from the K-Pg impact. ACP, 16(20), 13185-13212.

2.1. Impact-driven aerosol injection: Dust

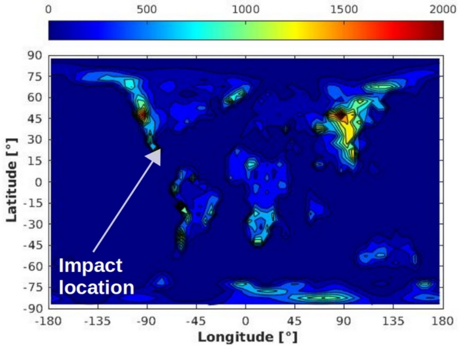

Terrain elevation map [m]

Dust-generated impact winter

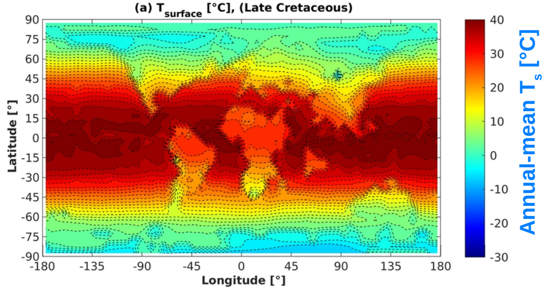

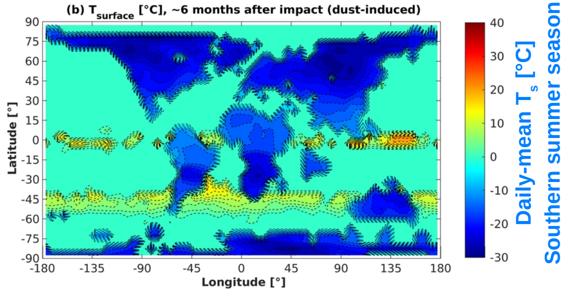

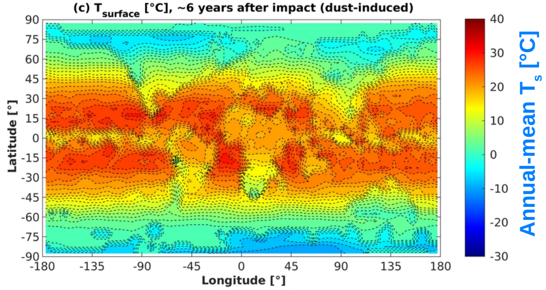

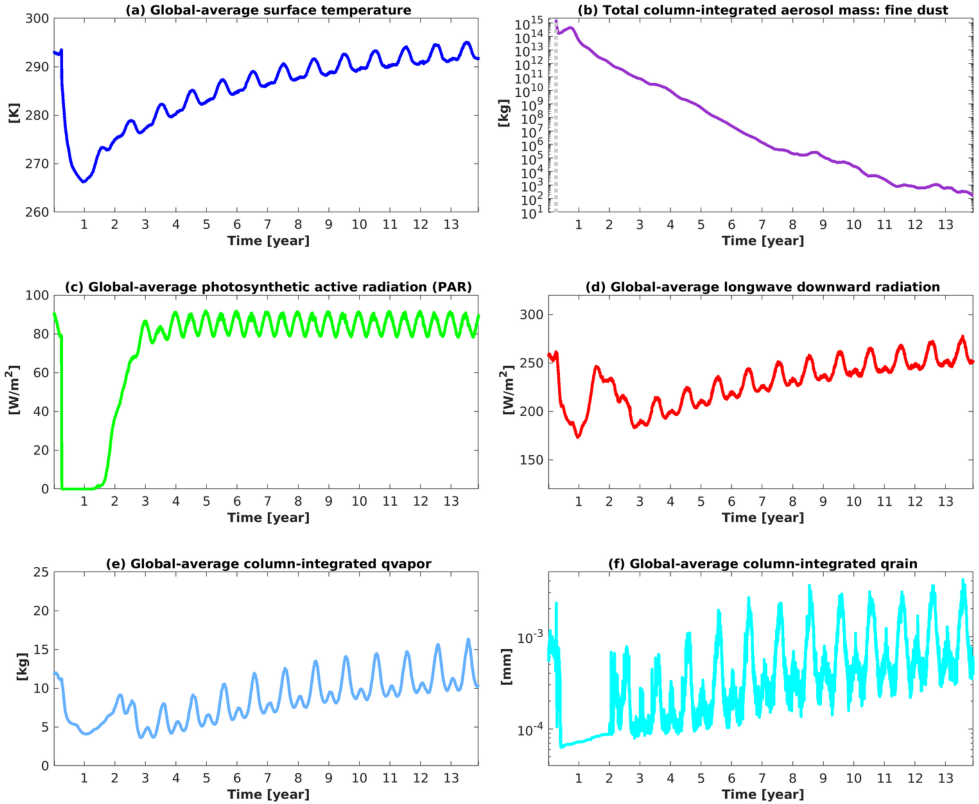

2.2. Impact-driven aerosol injection: Sulfur

13188 O. B. Toon et al.: Designing climate and chemistry simulations for asteroid impacts

Table 1. K-Pg injection scenario for impactor mass $\sim 1.4 \times 10^{18}$ g; impact energy $\sim 2.8 \times 10^{23}$ J $= 6.8 \times 10^{7}$ Mt for 20 km s^{-1} impact.

Property/ constituent	Type 2 spherules	Soot	Nanoparticles	Clastics, < µm	S
Material amount, g, column density (g cm^{-2})	2.3×10^{18} (0.44)	1.5–5.6 $\times 10^{16}$ (0.29 to 1.1 $\times 10^{-2}$)[c]	$\sim 2 \times 10^{18}$[b] (0.4)	$< 6 \times 10^{16}$ (0.01)	9×10^{16} (5×10^{-2} g cm^{-2} as SO_4)
Global optical depth as 1 µm particles[a]	∼ 20 (for 250 µm particles)	∼ 100	∼ 2000	∼ 90	∼ 450
Vertical distribution	70 km, Gaussian distribution with half width of 6.6 km[d]	Eq. (2)	Same as Type 2 spherules	Uniformly mixed vertically above tropopause	Same as Type 2 spherules
Optical properties	Not relevant	$n = 1.8$ $k = 0.67$	Hervig et al. (2009)	Orofino et al. (1998) limestone	Sulfuric acid
Initial particle size	250 µm diameter	Lognormal, $r_m = 0.11$ µm, $\sigma = 1.6$; monomers 30–60 nm	20 nm diameter	Lognormal, $r_m = 0.5$ µm, $\sigma = 1.65$	Gas
Material density, g cm^{-3}	2.7	1.8	2.7	2.7	1.8

[a] Qualitative estimate for comparison purposes only. [b] This value is an upper limit. The lower limit is zero. [c] These values are for aciniform soot or elemental carbon in the stratosphere (see text). [d] The material may have quickly moved to below 50 km to maintain hydrostatic balance (see text).

- **Injected sulfur mass:**

  325,000 Tg → sulfur
  650,000 Tg → SO_2
  based on the hydrocode simulations by Artemieva et al. (2017)

- No photochemistry of SO_2 → H_2SO_4 conversion

Toon, O. B., Bardeen, C., & Garcia, R. (2016). Designing global climate and atmospheric chemistry simulations for 1 and 10 km diameter asteroid impacts using the properties of ejecta from the K-Pg impact. Atmospheric Chemistry and Physics, 16(20), 13185-13212.

2.2. Impact-driven aerosol injection: Sulfur

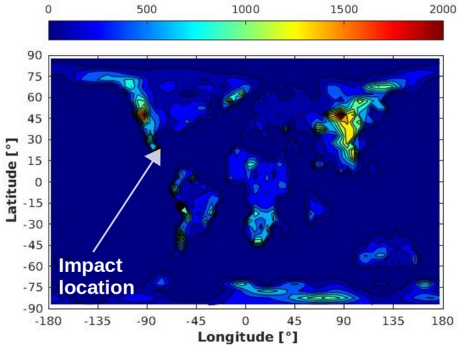

Terrain elevation map [m]

Sulfur-generated impact winter

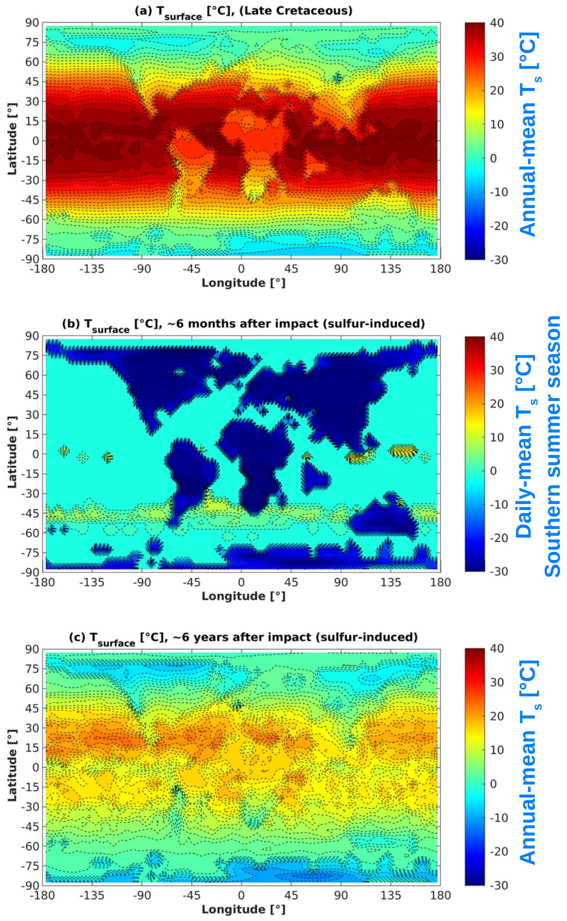

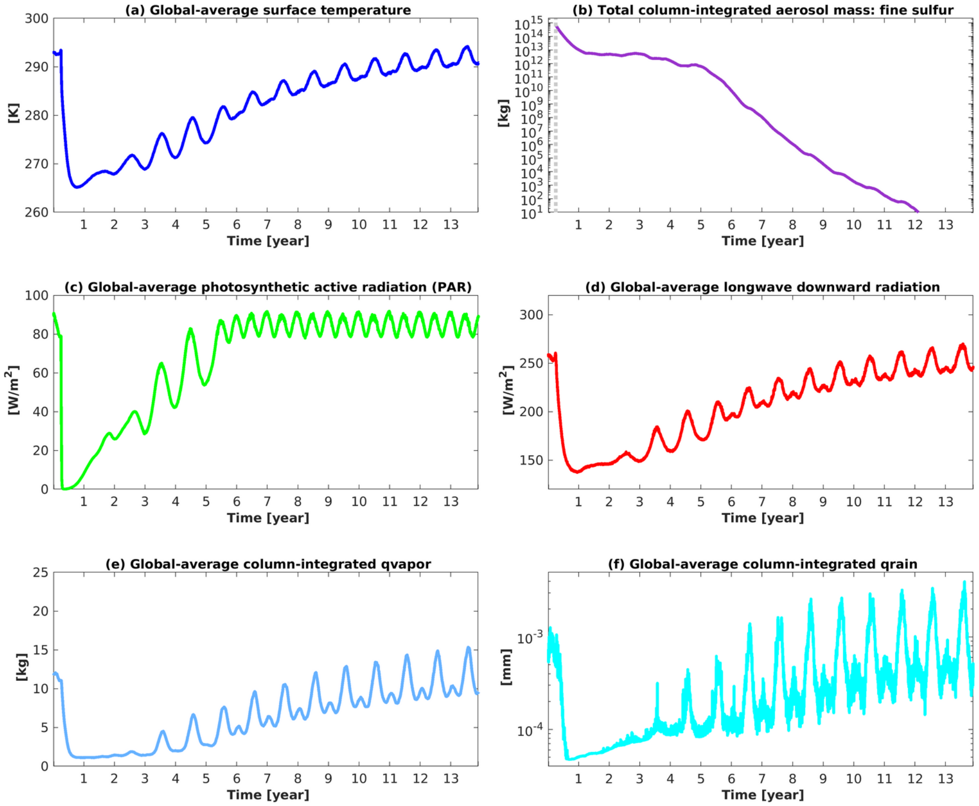

2.3. Impact-driven aerosol injection: Fine soot

13188 O. B. Toon et al.: Designing climate and chemistry simulations for asteroid impacts

Table 1. K-Pg injection scenario for impactor mass $\sim 1.4 \times 10^{18}$ g; impact energy $\sim 2.8 \times 10^{23}$ J $= 6.8 \times 10^7$ Mt for 20 km s^{-1} impact.

Property/ constituent	Type 2 spherules	Soot	Nanoparticles	Clastics, < µm	S
Material amount, g, column density (g cm^{-2})	2.3×10^{18} (0.44)	1.5–5.6 $\times 10^{16}$ (0.29 to 1.1×10^{-2})[c]	$\sim 2 \times 10^{18}$[b] (0.4)	$< 6 \times 10^{16}$ (0.01)	9×10^{16} (5×10^{-2} g cm^{-2} as SO_4)
Global optical depth as 1 µm particles[a]	~20 (for 250 µm particles)	~100	~2000	~90	~450
Vertical distribution	70 km, Gaussian distribution with half width of 6.6 km[d]	Eq. (2)	Same as Type 2 spherules	Uniformly mixed vertically above tropopause	Same as Type 2 spherules
Optical properties	Not relevant	$n = 1.8$ $k = 0.67$	Hervig et al. (2009)	Orofino et al. (1998) limestone	Sulfuric acid
Initial particle size	250 µm diameter	Lognormal, $r_m = 0.11$ µm, $\sigma = 1.6$; monomers 30–60 nm	20 nm diameter	Lognormal, $r_m = 0.5$ µm, $\sigma = 1.65$	Gas
Material density, g cm^{-3}	2.7	1.8	2.7	2.7	1.8

[a] Qualitative estimate for comparison purposes only. [b] This value is an upper limit. The lower limit is zero. [c] These values are for aciniform soot or elemental carbon in the stratosphere (see text). [d] The material may have quickly moved to below 50 km to maintain hydrostatic balance (see text).

Aerosol log-normal particle size distribution

$$n_N(D_p)dD_p = \frac{1}{\sqrt{2\pi} D_p ln\sigma_{g,0}} exp\left(-\frac{(lnD_p - lnD_{pg,0})^2}{2ln^2\sigma_{g,0}}\right)$$

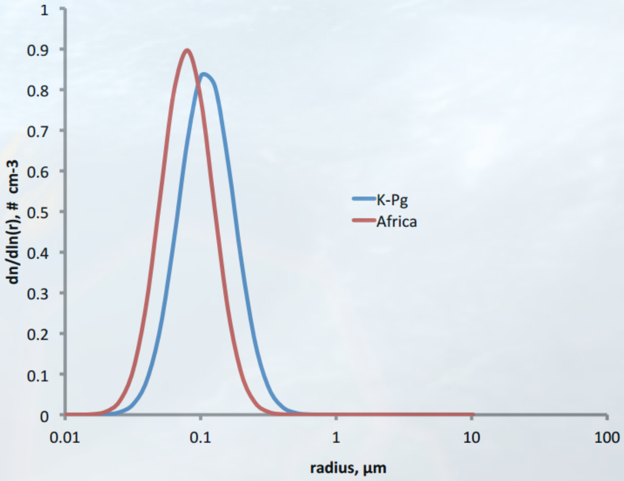

Figure 2. The size distributions for smoke from modern fires in Africa and from the K-Pg boundary layer (Wolbach et al., 1985; Matichuk et al., 2008).

Toon, O. B., Bardeen, C., & Garcia, R. (2016). Designing global climate and atmospheric chemistry simulations for 1 and 10 km diameter asteroid impacts using the properties of ejecta from the K-Pg impact. Atmospheric Chemistry and Physics, 16(20), 13185-13212.

2.3. Impact-driven aerosol injection: Fine soot

Soot: coarse vs. fine black carbon injection.

666 ARTICLES NATURE VOL. 334 25 AUGUST 198

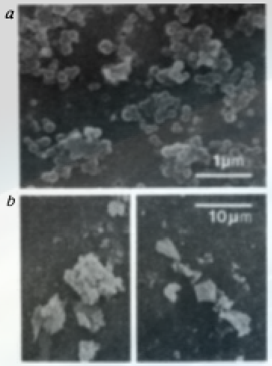

Fig. 1 Morphology of K-T carbon. *a*, Soot of characteristic 'grape bunch' morphology dominates in boundary clay (0.3–0.4 cm above boundary). *b*, Irregularly shaped, platey or pitted coarse carbon, presumably charcoal, dominates at higher levels (17.4–19.9 and 3.6–5.8 cm). Unlike soot, which forms only in flames[48], charcoal forms at lower temperatures, by charring and devolatilization of fuel. All samples were etched with dichromate to remove kerogen.

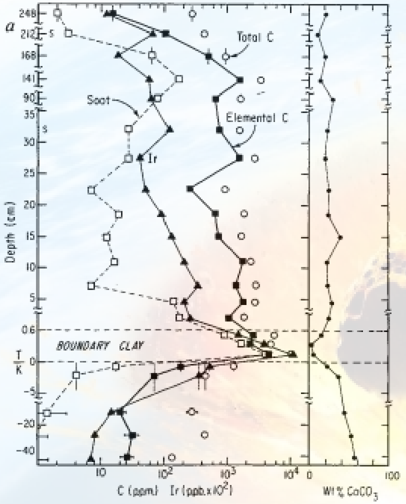

difference) as well as the content of insoluble minerals. The elemental C was examined by scanning electron microscope (SEM) and the mass fraction of soot was found by planimetric analysis[13].

Carbon and iridium profiles at boundary

Figure 2*a* shows the data for the ~3-m section straddling the boundary, with the −5 to +35 cm and especially the 0 to +0.6 cm intervals expanded. No corrections for carbonate content were made. Iridium and elemental C concentrations both rise sharply at the boundary, by factors of 1,500 and 210 compared with the Cretaceous average of 0.076 parts per 10^9 (p.p.b.) and 22 p.p.m. Both reach their maximum in the basal 0.3 cm of the boundary clay and decline afterwards, but the decline for Ir is greater and more regular. Soot, with a Cretaceous average of 1±0.5 p.p.m., shows an even steeper rise (×3,600) in the basal layer and becomes a major component (up to 71%) of the elemental C in the boundary clay, as shown by the convergence of the two curves. It then declines sharply, becoming a minor (<1 to 16%) component of the elemental carbon. All three curves revert to Cretaceous levels only at ~250 cm.

The large, abrupt rise in C and Ir at Woodside Creek is not unique. The Chancet Rocks site, 15 km away, shows a similar increase (Fig. 2*b*). Although this site is tectonically disturbed[10] and lacks boundary clay in places, it too shows a steep rise in elemental C and Ir at the boundary, by factors of 3×10^5 and 290 respectively.

The rise in C at Chancet Rocks may have been exaggerated by local geological factors. Still, it is curious that our earlier data for the Danish K-T boundary—the only place for which

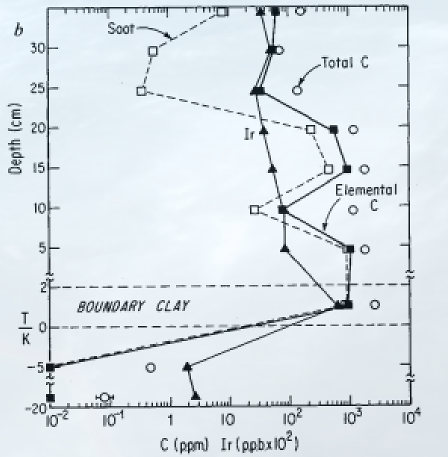

Fig. 2 Carbon and Ir profiles at the K-T boundary. *a*, At Woodside Creek the concentrations of Ir, elemental C and especially soot rise steeply at the boundary, by factors of 1,500, 210 and 3,600. Soot appears in the first 0.3 cm interval of the boundary clay, showing that fires started before the fallout had settled. After an initial drop above the boundary, all three decline gradually.

Injected coarse/fine soot: 72,700 Tg (Tabor et al., 2020)*

"Emission of 72,700 Tg of carbon from the global fires with 28.6% of that total emitted as fine soot come from measurements of elemental carbon found in KPB clays (Wolbach et al., 1990, 2003)"

*Tabor, C. R., Bardeen, C. G., Otto-Bliesner, B. L., Garcia, R. R., & Toon, O. B. (2020). Causes and climatic consequences of the impact winter at the Cretaceous-Paleogene boundary. Geophysical Research Letters, 47(3), e60121.

2.3. Impact-driven aerosol injection: Fine soot

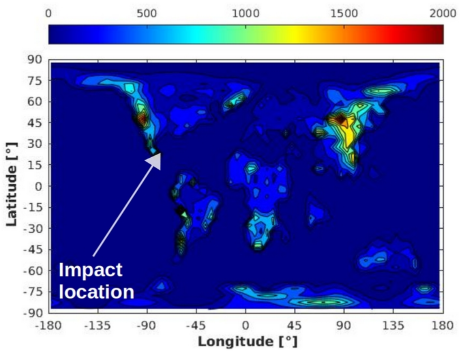

Terrain elevation map [m]

Soot-generated impact winter

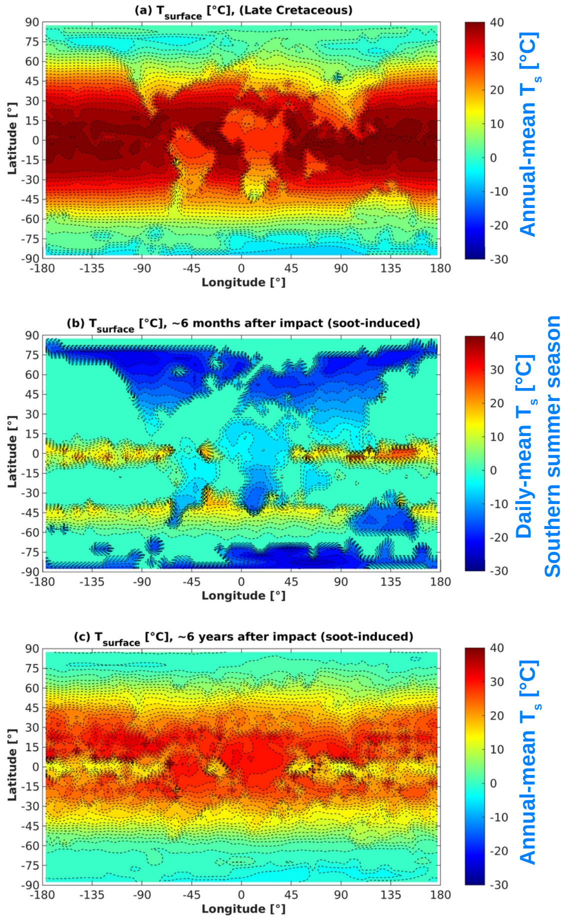

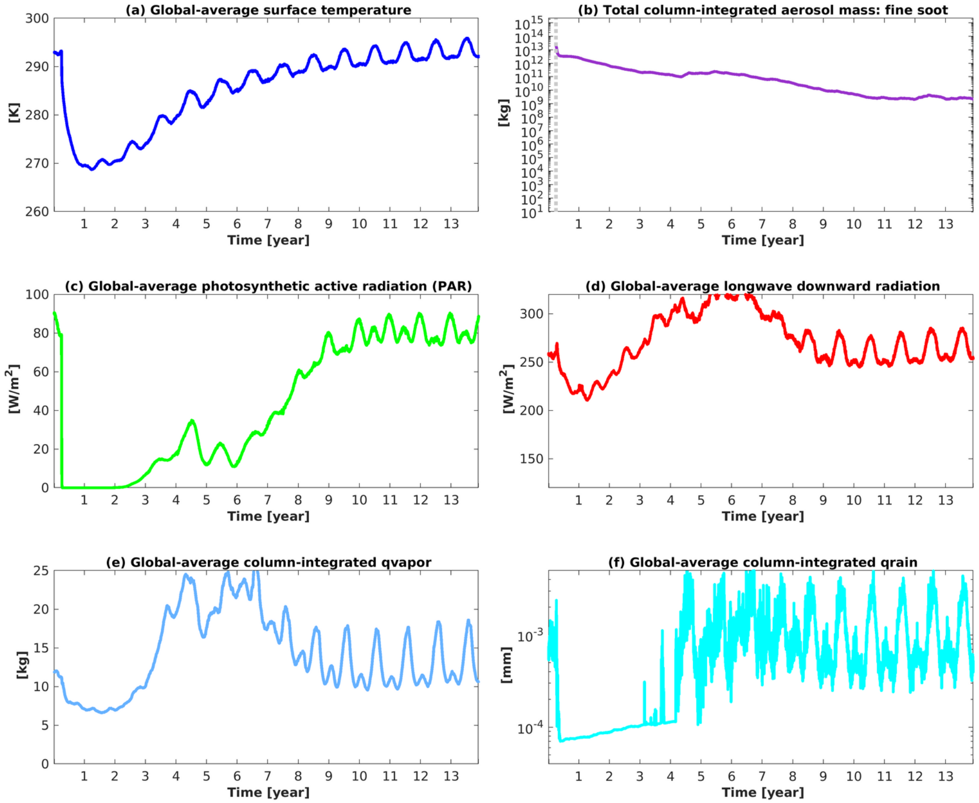

3. Conclusion & Next step

Quantifying photosynthetically active radiation (PAR) flux reduction following the K-Pg impact.

email: **cem.berk@observatory.be**

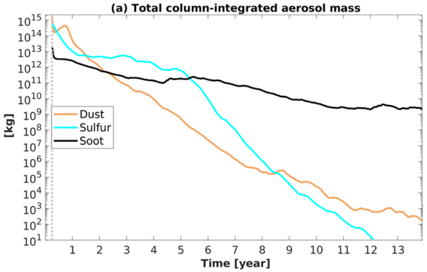

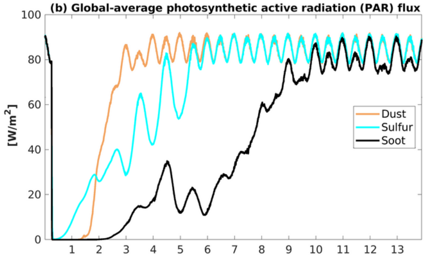

Next Step:
Combined impact scenario
Dust+Sulfur+Fine Soot

Annual-mean | **Daily-mean, 2^{nd} day post-impact** | **Daily-mean, 365^{th} day post-impact** | **Daily-mean, 700^{th} day post-impact**

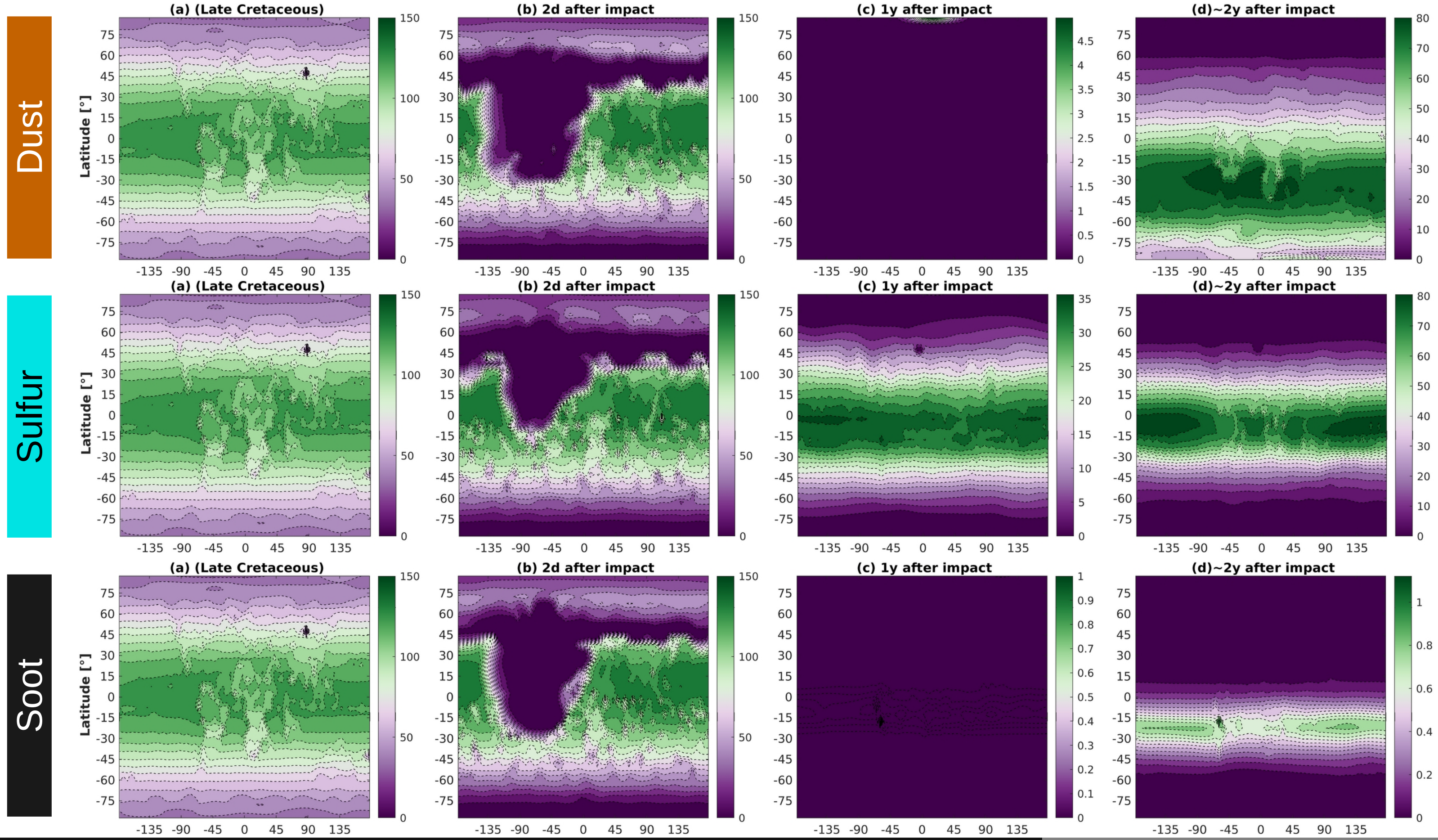

References

Toon, O. B., Zahnle, K., Morrison, D., Turco, R. P., & Covey, C. (1997). Environmental perturbations caused by the impacts of asteroids and comets. Reviews of Geophysics, 35(1), 41-78.

Toon, Owen B., Charles Bardeen, and Rolando Garcia. "Designing global climate and atmospheric chemistry simulations for 1 and 10 km diameter asteroid impacts using the properties of ejecta from the K-Pg impact." Atmospheric Chemistry and Physics 16.20 (2016): 13185-13212.

Upchurch Jr, G. R., Kiehl, J., Shields, C., Scherer, J., & Scotese, C. (2015). Latitudinal temperature gradients and high-latitude temperatures during the latest Cretaceous: Congruence of geologic data and climate models. Geology, 43(8), 683-686.

Niezgodzki, I., Knorr, G., Lohmann, G., Tyszka, J., & Markwick, P. J. (2017). Late Cretaceous climate simulations with different CO2 levels and subarctic gateway configurations: A model-data comparison. Paleoceanography, 32(9), 980-998.

Tabor, C. R., Bardeen, C. G., Otto-Bliesner, B. L., Garcia, R. R., & Toon, O. B. (2020). Causes and climatic consequences of the impact winter at the Cretaceous-Paleogene boundary. Geophysical Research Letters, 47(3), e60121.

Vellekoop, J., Sluijs, A., Smit, J., Schouten, S., Weijers, J. W., Damsté, J. S. S., & Brinkhuis, H. (2014). Rapid short-term cooling following the Chicxulub impact at the Cretaceous–Paleogene boundary. Proceedings of the National Academy of Sciences, 111(21), 7537-7541.

Brugger, J., Feulner, G., & Petri, S. (2017). Baby, it's cold outside: Climate model simulations of the effects of the asteroid impact at the end of the Cretaceous. Geophysical Research Letters, 44(1), 419-427.

Senel, C. B., Temel, O., Porchetta, S., Muñoz-Esparza, D., & van Beeck, J. (2019). A new planetary boundary layer scheme based on LES: Application to the XPIA campaign. Journal of Advances in Modeling Earth Systems, 11(8), 2655-2679.

Senel, C. B., Temel, O., Lee, C., Newman, C. E., Mischna, M. A., Muñoz-Esparza, D., et al. (2021). Inter-annual, seasonal and regional variations in the Martian convective boundary layer derived from GCM simulations with a semi-interactive dust transport model. Journal of Geophysical Research: Planets, 126, e2021JE006965.

Lim, K. S. S., & Hong, S. Y. (2010). Development of an effective double-moment cloud microphysics scheme with prognostic cloud condensation nuclei (CCN) for weather and climate models. Monthly weather review, 138(5), 1587-1612.

Dudhia, J. (1996, July). A multi-layer soil temperature model for MM5. In Preprints, The Sixth PSU/NCAR mesoscale model users’ workshop (pp. 22-24).

Shao, Y. (2001). A model for mineral dust emission. Journal of Geophysical Research: Atmospheres, 106(D17), 20239-20254.

Shao, Y. (2004). Simplification of a dust emission scheme and comparison with data. Journal of Geophysical Research: Atmospheres, 109(D10).

Shao, Y., Ishizuka, M., Mikami, M., & Leys, J. F. (2011). Parameterization of size-resolved dust emission and validation with measurements. Journal of Geophysical Research: Atmospheres, 116(D8).

Richardson, M. I., Toigo, A. D., & Newman, C. E. (2007). PlanetWRF: A general purpose, local to global numerical model for planetary atmospheric and climate dynamics. Journal of Geophysical Research: Planets, 112(E9).

Pollard, R. T., Rhines, P. B., & Thompson, R. O. (1973). The deepening of the wind-mixed layer. Geophysical Fluid Dynamics, 4(4), 381-404.

Chou, M. D., & Suarez, M. J. (1999). A solar radiation parameterization for atmospheric studies (Vol. 15, p. 38). National Aeronautics and Space Administration, Goddard Space Flight Center, Laboratory for Atmospheres, Climate and Radiation Branch.

Chou, M. D., Suarez, M. J., Liang, X. Z., Yan, M. M. H., & Cote, C. (2001). A thermal infrared radiation parameterization for atmospheric studies.